A Comparison of Measured and Predicted XV-15 Tiltrotor Surface Acoustic Pressures

Karen H. Lyle
Aerospace Engineer, US Army Vehicle Technology Center
Hampton, VA

Casey L. Burley
Aerospace Engineer, NASA Langley Research Center
Hampton, VA

Devon S. Prichard
Aerospace Engineer, Lockheed Martin Engineering and Sciences Corporation
Hampton, VA

Abstract

Predicted XV-15 exterior surface acoustic pressures are compared with previously published experimental data. Surface acoustic pressure transducers were concentrated near the tip-path-plane of the rotor in airplane mode. The comparison emphasized cruise conditions which are of interest for tiltrotor interior noise - level flight for speeds ranging from 72 m/s to 113 m/s. The predictions were produced by components of the NASA Langley Tiltrotor Aeroacoustic Code (TRAC) system of computer codes. Comparisons between measurements and predictions were made in both the time and frequency domains, as well as overall sound pressure levels. In general, the predictions replicated the measured data well. Discrepancies between measurements and predictions were noted. Some of the discrepancies were due to poor correlation of the measured data with the rotor tach signal. In other cases limitations of the predictive methodology have been indicated.

Introduction

Tiltrotor aircraft are being proposed as a viable means of intercity travel. The tiltrotor is able to pick up passengers at the center of a city and then transport them relatively quickly to locations within a 500 kilometer radius. In order for such vehicles to be commercially viable, the interior noise and vibration levels must be acceptable to the general public as passengers. A review of the literature revealed very little structural-acoustic data or predictions related to the tiltrotor and more specifically to the XV-15. Shank[1] reported that the measured untreated tiltrotor interior noise levels are comparable to helicopters for hover; however, in forward flight the tiltrotor is somewhat quieter than helicopters. In addition to the data presented by Shank, a memo written by Maisel[2] includes exterior spectral levels measured on the surface of the XV-15 at four positions, as well as information regarding the repeatability and stability of such measurements. However, Maisel's data are neither formally documented nor generally available. Additional data are necessary to better understand the physical mechanisms that produce the structural vibrations and interior noise in the tiltrotor. This paper focuses on development of a predictive methodology for the surface acoustic pressures on the fuselage skin. Predictions are compared with previously published measured data[3]. Although the data presented in this article are limited to the exterior surface pressures during level flight in airplane mode, the complete measured data set also included structural accelerations and interior pressures for both level flight in airplane mode and out-of-ground-effect (OGE) hover in helicopter mode flight conditions.

Test Description

The XV-15 is a prototype tiltrotor (three-bladed propeller), see Figure 1. A diagram of the XV-15 with transducer positions indicated

is shown in Figure 2. This particular aircraft was built in the early 1980's as a proof-of-concept for tiltrotor technology. A photograph indicating the transducer locations is shown in Figure 3, with position coordinates listed in Table I. These transducer positions form a "T" centered about Position A which was assumed *a priori* to be the closest approach of the port side propeller to the fuselage during airplane mode. Position D was located near the wing fairing, which caused considerable flow noise to be evident in the data. Position F was at the top center of the fuselage and would presumably see equal contributions from both rotors. The two rotors are mechanically linked so that they rotate at exactly the same rate. This eliminates any 'beating' in the signals but also eliminates the capability to distinguish the response of the two rotors. In addition, the blades are synchronized such that if a blade is vertical on the left rotor, then the corresponding blade on the right rotor is also vertical.
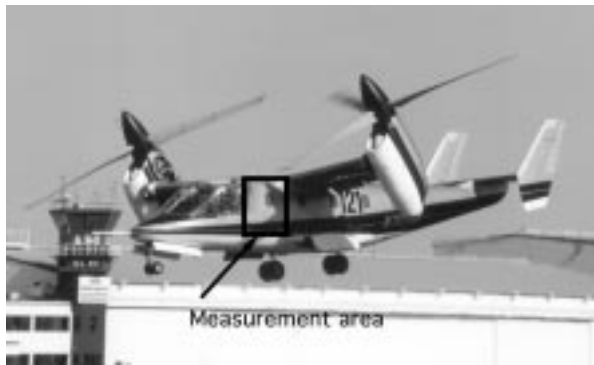
Figure 1. Photograph of XV-15.

The exterior pressures were measured at nine positions using surface mounted pressure transducers with 1.88 mm diameter diaphragms. The surface mount resulted in the transducer protruding approximately 1.5 mm from the skin (Figure 3 inset). The offset into the flow would contribute to high frequency self-noise. However, for the data presented in this paper, this offset into the flow was not considered critical due to the dominant low frequencies generated by the rotating blades and the relatively low forward flight speeds. These exterior pressure sensors measured differential pressures and were vented to the aircraft interior. The transducers were rated to

+/- 3450 Pa (differential) with a nominal sensitivity of 0.000261 mV/Pa/Vin. For this test the excitation voltage was 12 V. A signal conditioner provided a gain of 1100 to assure adequate input to the tape recorder. The static pressure differential was confirmed to be sufficiently low during post-test data analysis.
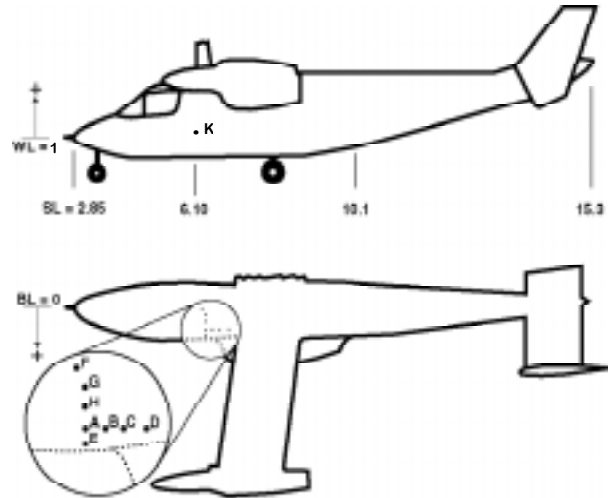
Figure 2. Diagram of XV-15 fuselage and transducer positions.
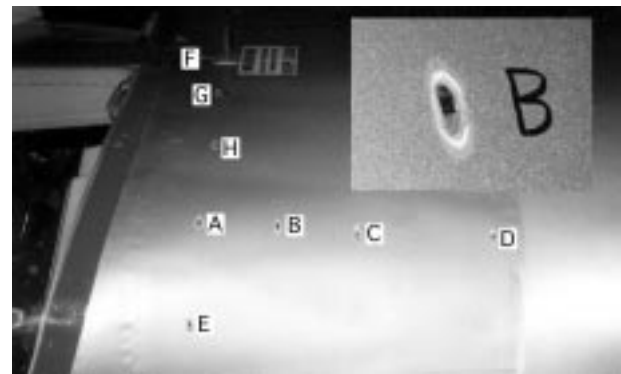
Figure 3. Photograph of sensor positions.

One minute of data was acquired at each of the five flight conditions indicated in Table II. The transducer signals as well as the rotor tach signal were recorded on a 32-channel digital tape recorder at a sampling rate of 5 kHz. The data were then downloaded to a computer workstation for data reduction and analysis. One hundred fifteen onboard data parameters

were simultaneously recorded for correlation with the transducer data via the recorded time code. Some of these parameter values, such as collective angle and aircraft altitude, have been included in the table.

Table I. Transducer locations in meters.

Location	Station-Line (SL)	Butt-Line (BL)	Water-Line (WL)
A	6.18	0.610	2.41
B	6.32	0.597	2.40
C	6.45	0.584	2.39
D	6.69	0.572	2.37
E	6.18	0.737	2.31
F	6.12	0.0	2.46
G	6.17	0.184	2.46
H	6.18	0.394	2.45
K	6.18	0.800	1.08

Table II. Test flight conditions.

	Condition				
	I	II	III	IV	V
Nacelle angle (deg.)	0	0	0	0	0
Flap Setting (deg.)	20.	0.0	0.0	0.0	0.0
Velocity (m/s)	72.0	82.2	92.5	103	113
Rotor speed (rpm)	523	523	523	523	523
Collective (deg.)	30.7	34.2	37.3	40.6	43.1
Angle of attack (deg.)	2.40	4.09	2.15	0.486	-0.475
Precone (deg.)	2.5	2.5	2.5	2.5	2.5
Aircraft altitude (m)	853	873	863	838	860
Amb. temp. (°C)	17.7	18.5	19.4	20.7	21.6
Amb. pressure (Pa)	9.1e04	9.1e04	9.1e04	9.2e04	9.1e04
Amb. density (kg/m^3)	1.09	1.09	1.08	1.08	1.08

Prediction Methodology

The Tiltrotor Aeroacoustic Code (TRAC)[4] was employed to predict the pressures on the fuselage surface. TRAC is currently being developed under the Short Haul (Civil Tiltrotor) program by NASA and the U.S.

helicopter industry. The purpose of TRAC is to provide aeroacoustic analysis for the design and evaluation of efficient low-noise tiltrotors as well as support for the development of safe, low-noise flight profiles. TRAC consists of several standalone codes providing comprehensive trim, unsteady 3-D subsonic and transonic aerodynamics, rotor source noise, and acoustic propagation. TRAC also has standardized input/output files and interface codes to assist in reformatting data between codes. A schematic of the TRAC codes employed for this paper are shown in Figure 4.

To perform a full aircraft noise prediction with TRAC, a description of the vehicle, including its aerodynamic properties (airfoil and body force and moment coefficient tables) must be given. The full aircraft rotor trim and performance may then be determined using the comprehensive rotorcraft analysis code CAMRAD.Mod1[5] [6]. The trimmed results, which include the rotor collective pitch setting and the "partial" angle-of-attack of the blade sections as a function of radial position are then utilized by the rotor CFD analysis FPXBVI[7] to compute the aerodynamic flowfield surrounding an isolated blade. The flowfield solution is then used by PANIC (Propeller Acoustic Nearfield Interpolation Code) to estimate the fuselage wall acoustic pressure time histories. These time histories are then compared to measurements.

As seen in Figure 4, other codes are included in the prediction procedure, namely, FPRBVI and GRIDMOD. These codes were used to generate and tailor a CFD grid appropriate for computing accurate pressures to the outer boundary of the grid (far from the blade surface). The built-in grid generator in the FPRBVI[8] rotor CFD code was used to generate an initial blade-fitted O-H grid. Typically, these grids are most dense near the blade surface and become coarser in the normal direction to the blade surface. For the current problem, where the solution is desired away from the blade surface, it is important to ensure that the grid density is appropriately dense throughout the grid to maintain solution accuracy. To achieve this, the grid was modified using a new code called GRIDMOD (GRID MODification), which was developed specifically for this study. Details of the grid

modifications as well as the prediction methodology follow.
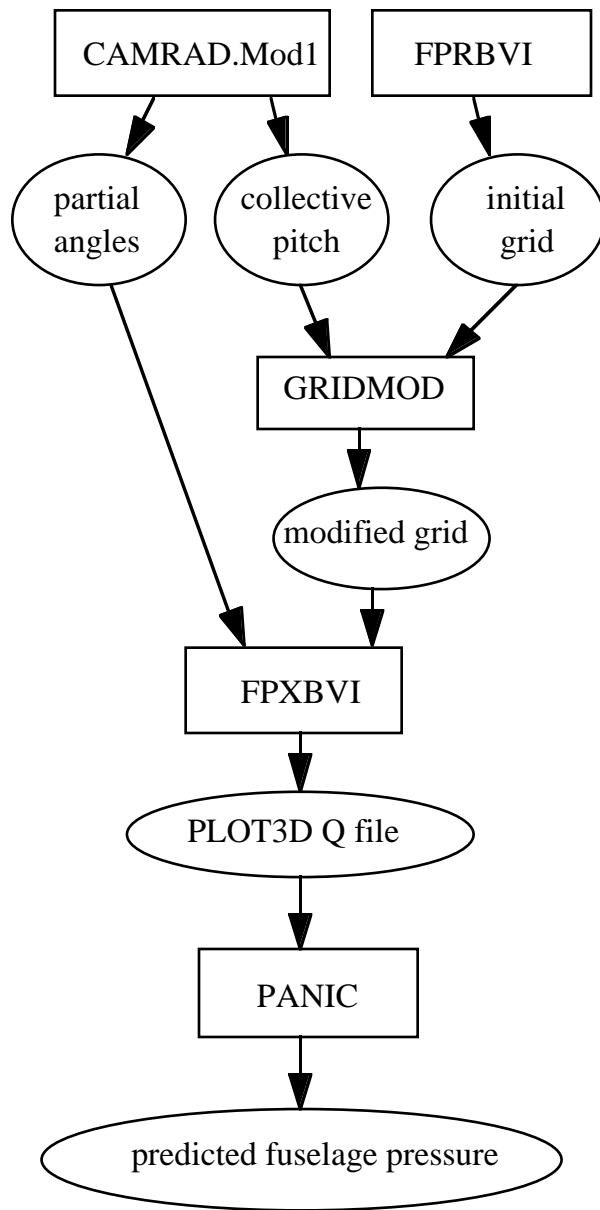
Figure 4. Schematic of TRAC version used for the prediction of fuselage pressures.

CAMRAD.Mod1: The CAMRAD.Mod1 program, an extension of the original CAMRAD code, was developed at NASA Langley. It performs trim, performance, aerodynamic, and aeroelastic calculations for arbitrary rotorcraft (including tiltrotors). The wing-body-tail aircraft aerodynamics were modeled in CAMRAD.Mod1 using the recently developed option which utilizes an empirical table look-up for the body aerodynamics. The aerodynamic lift, drag, and moment of the combined wing, fuselage and tail surfaces were tabulated as functions of aircraft pitch and Mach number. A prescribed wake was employed with 10 degrees of azimuthal resolution. Four bending modes and 2 torsion modes were used to model the blade motions. The partial angles-of-attack (which include effects of blade twist, pitch, flapping velocity, rotor rotation, freestream, and part of the wake-induced inflow) were computed over the rotor disk and output for use in the FPXBVI code. These partial angles allowed for more accurate modeling of the local blade flow during the FPXBVI computations.

The aircraft was trimmed in the analysis to symmetric, level flight at each given airspeed, by adjusting the control settings and aircraft attitude. The results of the predicted aircraft trim are summarized in Table III. Comparison of the predicted collective values with those of the measured values show that the predicted values are consistently about 4 degrees low. The predicted pitch attitude of the aircraft, however, was found to be on the order of 3 degrees greater than that of the measured values. The differences between measured and predicted values are attributed in part to the accuracy of the tables used to define the aerodynamics of the aircraft body.

The predicted performance of the XV-15 aircraft is shown in Figure 5 for cruise flight. The rotor propulsive efficiency is shown as a function of thrust and is compared to published full scale wind-tunnel test results[9][10]. The rotor propulsive efficiency η is defined by Johnson in Ref. [10] as $\eta = T \bullet V/P$, where T is the rotor thrust, V is the wind speed and P is the rotor power. The predicted efficiency correlates well with the measured full scale wind-tunnel results. This implies the global performance prediction by CAMRAD.Mod1 is good, although predicted details, such as collective, do not correlate well with measurements.

4

Table III. Comparison of predicted aircraft trim parameters.

	Condition				
	I	II	III	IV	V
Collective (deg.)					
measured	30.7	34.2	37.3	40.6	43.1
predicted	27.5	30.5	33.7	36.5	39.2
Angle of attack (deg.)					
measured	2.4	4.1	2.2	0.49	-.48
predicted	6.4	6.9	5.1	3.7	2.6

Test	V / WR	M_{tip}
○	0.34	0.53
□	0.365	0.65
◇	0.385	0.62
△	0.42	0.64
▽	0.45	0.60
◇	0.46	0.53
⬠	0.53	0.52
⬡	0.56	0.44
⬡	0.63	0.43
⬡	0.68	0.35
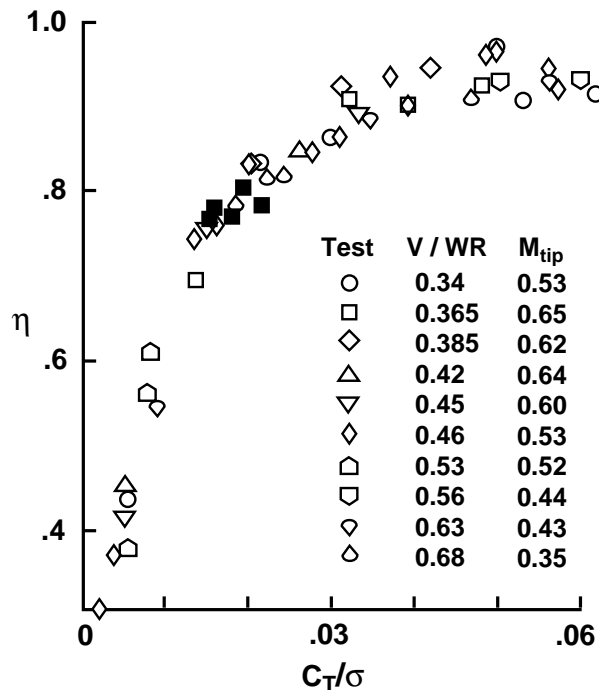
Figure 5. Comparison of wind-tunnel test and predicted (solid-squares) rotor propulsive efficiencies as a function of thrust (Ref. [9, 10]).

GRIDMOD: The initial grid generated by the built-in grid generation routines in FPRBVI was a body-fitted O-H grid consisting of flat O-planes stacked in the radial direction. Since the acoustic pressure was desired away from the blade as well as near it, the grid point distribution in the normal direction was modified to improve the spatial resolution away from the blade. In addition, the radial grid planes were "rotorized," i.e. relocated to a circular plane centered on the rotor's axis of rotation. This allows for a more accurate prediction of the fuselage pressures since the trajectories of the fuselage transducer locations in the blade reference frame follow a circular path. This also aligned each grid O-plane with the local rotational velocity vector. The overall flow is helical, thus the location of the branch cut in the full potential solution of FPXBVI had to be carefully handled. A method for reshaping the grid's branch cut into an approximately helical shape was added to GRIDMOD, such that the branch cut was more closely aligned with the flow. The collective pitch setting of the rotor was large (greater than 15 degrees, see Table III) so the collective pitch angle was added to the grid and removed from the partial angle-of-attack table from CAMRAD.Mod1. Lastly, since the location of the blade relative to the transducers is crucial to properly capturing the thickness noise effect, the effect of the 2.5 degree precone of the rotor blades was included in the grid for Conditions I and II in this paper.

FPXBVI: The flowfield about an isolated rotor blade was predicted using the FPXBVI full potential rotor CFD code. FPXBVI[11] is a joint AFDD/Langley development, and is the latest of the "FP" series of transonic full potential rotor CFD codes. In using this code, several assumptions about the relationship between the blade aerodynamics and the pressure on the fuselage were made. Only the deterministic aerodynamic pressure of the blade passage was considered; no turbulence, fuselage aerodynamic effects, or transducer self-noise were computed. Since the proprotors were in propeller mode, the aerodynamic calculation was made assuming perfectly axial flight, so that a more rapid steady calculation could be used instead of a longer unsteady calculation. The calculations presented were performed with a grid of 101 x 48 x 48 points in the wraparound, radial, and normal directions, respectively. The number of time steps used was 1200, to ensure a converged solution. The quasi-steady calculations were very sensitive to the flight conditions. For Conditions III, IV, and V the geometric effect of the blade precone was not included in the grid, since the solution would not converge for these cases. This will mainly affect the description of the blade location relative to the

fuselage transducer; the coning angle is small (2.5°), but may induce errors due to the highly directional nature of thickness noise. In addition a 'non-rotorized' grid was used for Conditions IV and V. The FPXBVI code would not converge completely when the 'rotorized' grid was used for these conditions.

The predictions performed using the CFD code were found to be more sensitive to the grid for propeller mode calculations than for helicopter mode calculations. Exact reasons for this are not completely understood at this time. However several factors contribute to the difficulties, including, the branch cut and its position relative to the flow, the generation of an appropriate grid, and accurate description of the aircraft trim and blade motion.

PANIC: Once the flow field of the isolated blade was determined, PANIC was utilized to compute an estimate of the fuselage wall acoustic pressure. PANIC calculates the trajectory of the transducer locations in the blade reference frame for a sequence of time steps (each corresponding to a new blade azimuthal position), then interpolates density at each time step for each fuselage transducer location. The aerodynamic pressure was obtained from the density by using an isentropic relation. Since there was not any substantial regions of supersonic flow in these calculations, the assumption of isentropic flow is reasonable. The freestream pressure was subtracted from the local pressure, yielding the acoustic pressure. By stepping through 120 degrees of blade travel, the acoustic pressure time history was developed for one blade passage. Blade-to-blade variations and blade interactions were not modeled, thus the time history was repeated for blades 2 and 3 to create a "one-rotor-rev" pressure time history. Figure 6 is an illustration of this process. In addition, only the effect of the port side rotor was considered. Diffraction and reflection effects were not considered, but are expected to increase the pressure amplitudes as frequency increases to a maximum of a pressure doubling. This method for estimating the wall acoustic pressure using a freefield solution is very approximate. However it is fairly easy to perform compared to a true 3-D multi-body acoustic analysis, and provides a useful design and analysis tool.
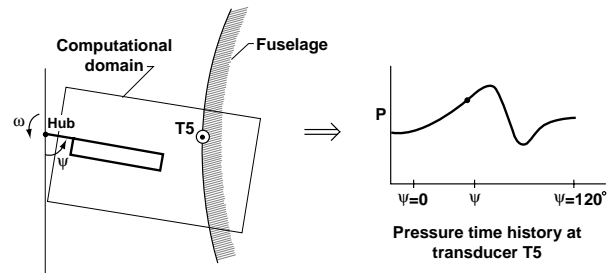
Figure 6. Illustration of determining an acoustic pressure time history on the fuselage of an aircraft from the FPXBVI full potential flow solution.

In summary, the approximations and assumptions made in the above method include;

- assumption of axial flow into the rotor;
- steady aerodynamic flow through the rotor;
- deterministic, isentropic, inviscid flow;
- the relative blade/transducer geometry is determined solely by the blade shape, collective pitch (for all conditions) and rotor precone (for Conditions I and II) - elastic deflections of the wing and rotor blades were neglected in the FPXBVI calculations;
- the spatial resolution of the grid was limited by the available grid generation tools and computational time available for the preparation of this paper;
- reflection and diffraction effects were not included in the analysis;
- FPXBVI predictions based on one rotor, while measurements had two;
- no blade-to-blade variations or blade interactions were modeled;
- acoustic predictions based on CAMRAD.Mod1 rotor trim conditions.

Results

Selection of results have been based on flight conditions, transducer positions and frequency range of interest for interior noise. Except where noted, the measured results are based on time-averaged results, synchronously averaged with the 1/rev rotor tach signal. Approximately 75 ensembles of exactly the same period were

averaged. A sample of the instantaneous and time-averaged response for Position A, Condition IV is shown in Figure 7. Most of the high frequency and broadband 'noise' has been eliminated by the averaging process. All of the predicted results are free-field calculations. In reality, the pressure on the fuselage should fall between the free-field and blocked pressures (or twice the free-field pressure). Correlations between measurements and predictions for Positions F and G will not be presented. The predictions were not considered reliable due to a number of factors including: the shallow incidence angle of the impinging pressure waves; the large numerical dissipation in the CFD solution due to greater wave travel distance; and the proximity of the transducer to the CFD grid boundaries.

Temporal Results

Sample comparisons between measured and predicted time histories are shown in Figure 8 and Figure 9. The data in Figure 8 are the response at the various transducer positions for Condition IV. The predictions track the measurements well in both pulse amplitude and duration. For instance, the measured and predicted responses for Positions A, E and K have a well defined negative pressure pulse of short duration. For Positions B, C, D and H,

this negative pulse is less defined for both measurements and predictions.
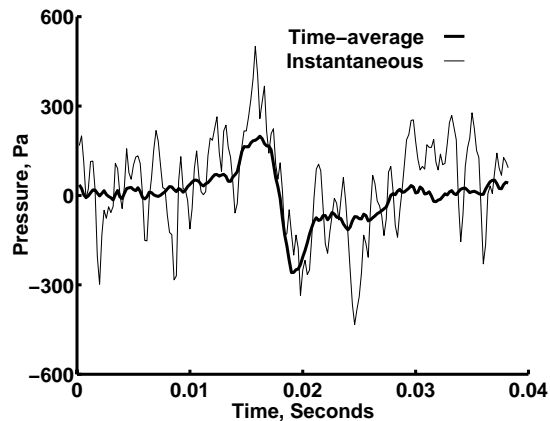
Figure 7. Instantaneous and time-averaged measured time history for Position A, Condition IV.

The effect of increasing the forward speed on the pressure is shown in Figure 9 for Position A. The predictions are consistently lower than the measurements for the peak overpressure for all the conditions at this position. Neglecting wave reflections and diffractions from the fuselage and inaccuracies in defining the relative blade/transducer geometry could contribute to the underprediction.
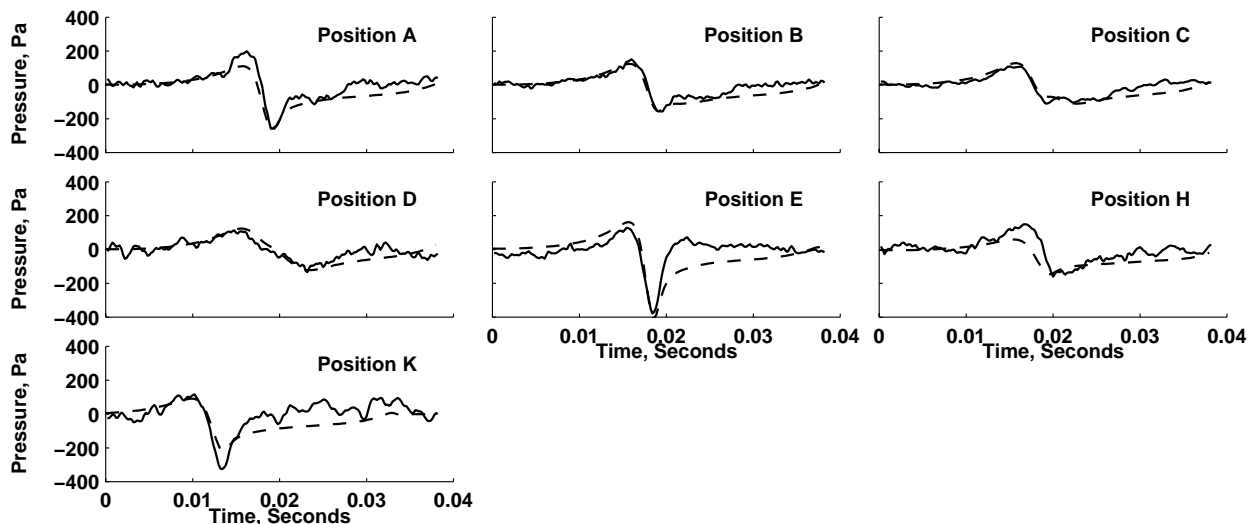
Figure 8. Comparison of measured and predicted time histories for Condition IV at 7 transducer positions (measured —, predicted ---).

7
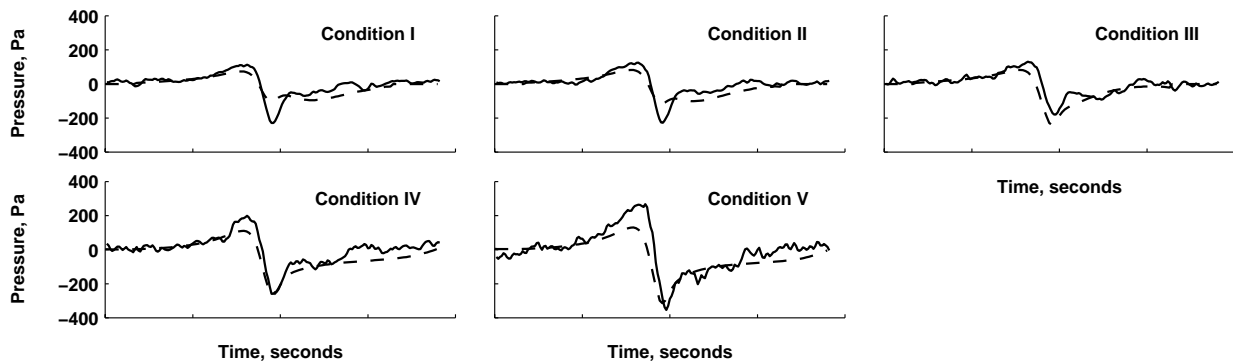
Figure 9. Comparison of measured and predicted time histories at Position A for 5 flight conditions (measured —, predicted ---).

Spectral Results

The data in Figure 8 and Figure 9 have been transformed to autospectra in Figure 10 and Figure 11, respectively. The first 10 harmonics of the blade passage frequency are shown. These frequencies were determined to be the primary contributor to the interior noise field, based on the interior noise microphone data that were included in Ref. [3]. Related coherence values are shown Figure 12. These coherences (relative to the 1/rev rotor tach signal) were calculated from the raw time data and not the synchronously time-averaged data. The circles indicate the average coherence for the 5 flight conditions, with the spread in coherence values indicated by the bars. In general, the coherence values are considered acceptable (greater than 0.5) for the first few harmonics at all the locations, except for the first harmonic at Position E. These coherence values provide insight as to the validity for comparing the measured data with a rotor prediction code. More specifically, a rotor prediction code would not be expected to predicted noise that is not correlated with rotor.

The autospectra for the first 10 harmonics for Condition IV are shown in Figure 10. Generally, the agreement between measured and predicted values is good. Both measured and predicted spectral levels decrease as a function of increasing frequency for

measurements at the out-of plane transducers, i.e., Positions A through D. These results indicate that the thickness noise, which is highly directional in-plane, tends to be the dominant noise source in the current configuration. Out-of-plane measurements and predictions show a decrease in levels, particularly at the higher frequencies. The higher harmonics of the in-plane positions, particularly E and K, remain more constant with frequency.

A comparison of measured and predicted autospectra for Position A as a function of flight condition have been plotted in Figure 11. The predictions agree very well with the measured data for the first 3 harmonics. However, TRAC significantly underpredicts the response at the higher harmonics for Conditions I and II. The larger discrepancy between measured and predicted spectra at the lower flight speeds could be due to the violation of the assumption of axial flow into the rotor at lower speeds (see Table III). The exact causes of the discrepancies seen for Condition V have yet to be determined.

A summary of the autospectra comparisons is shown in Figure 13. Each data point was calculated by averaging across frequency the absolute value of the difference between measured and predicted SPL. Note that the averages are based only on data where the average measured coherence is greater than 0.5. Considering the simplifying assumptions

of the prediction model, the agreement is remarkably good (less than 4 dB) for Conditions III-V at all the positions. For Conditions I and II, the difference between measured and predicted values ranged from 6 to 8 dB, except at Position D. The better agreement for Position D results from the limited number of frequencies used in the

average. Based on the coherence criteria, only values the from the first 3 harmonics are used. As seen in Figure 11, the predicted values agree well for the first 3 harmonics. These results are considered to be very good based on the level of modeling.
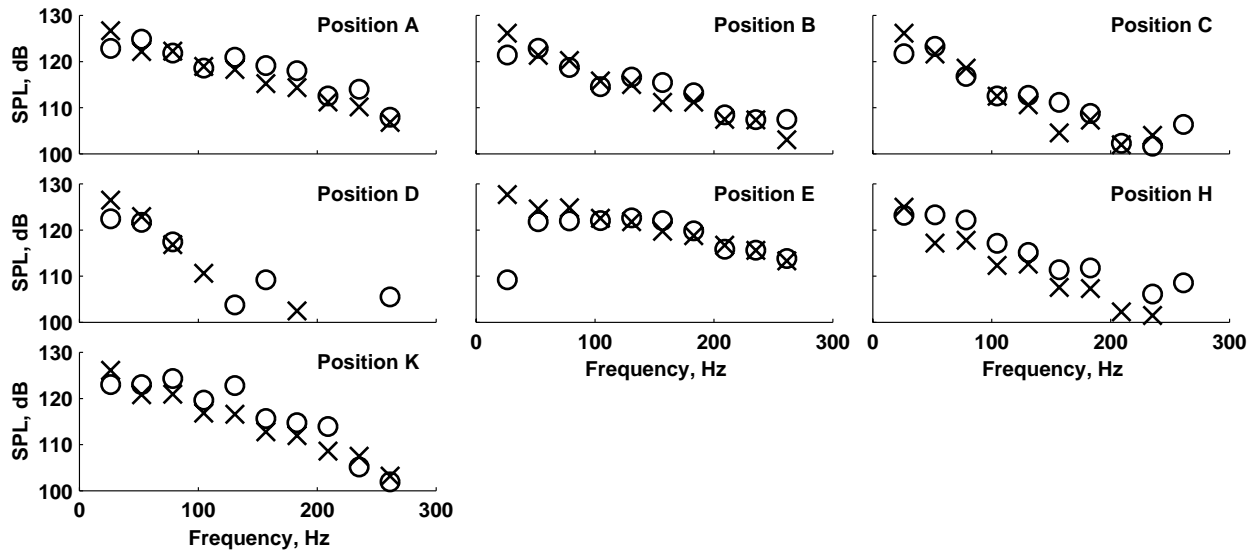
Figure 10. Comparison of measured and predicted pressure autospectra for Condition IV at 7 transducer positions (measured **O,** predicted ×).
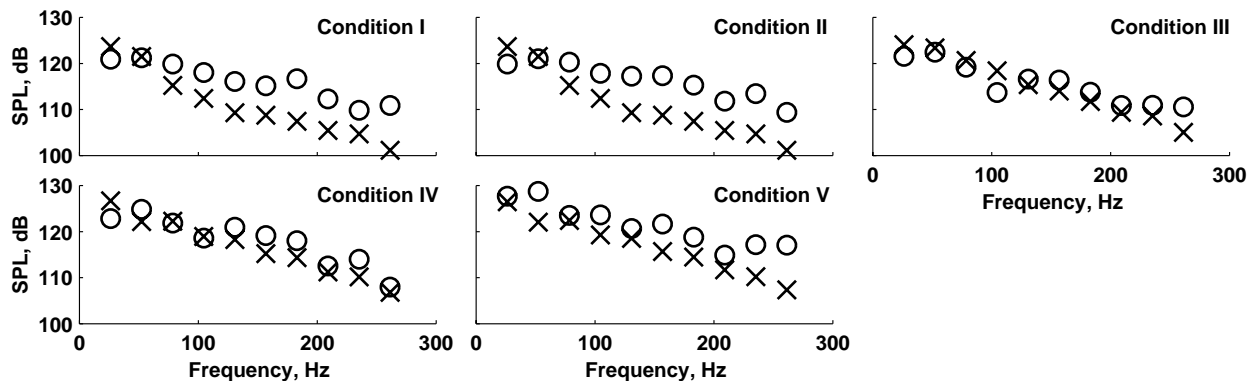
Figure 11 . Comparison of measured and predicted autospectra at Position A for 5 flight conditions (measured **O**, predicted ×).

9
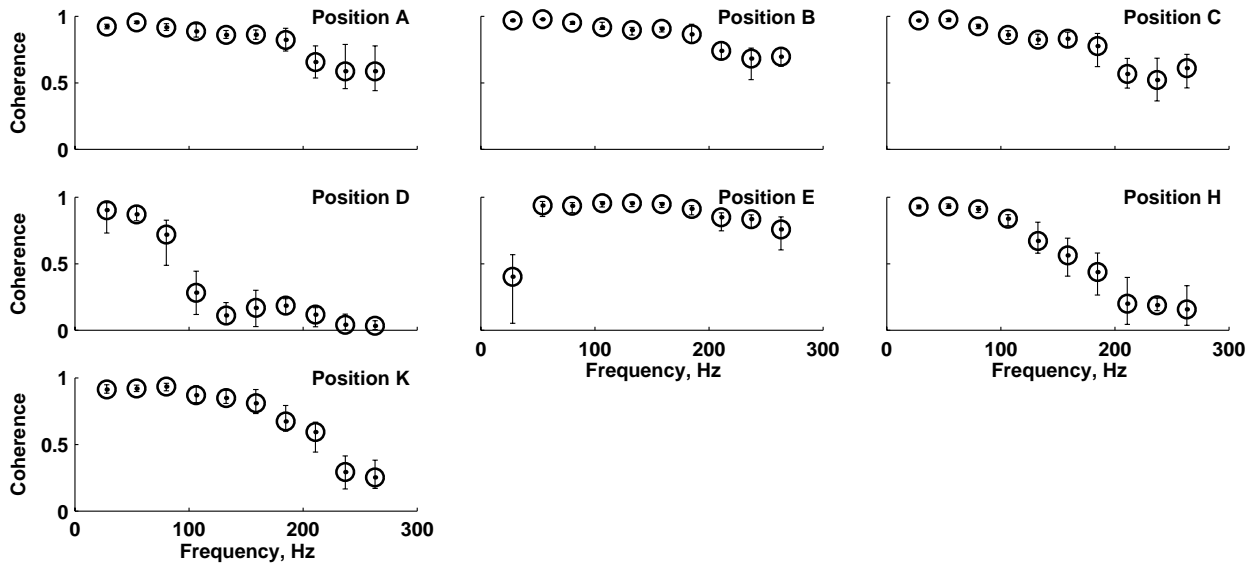
Figure 12. Measured coherence values for pressure transducers relative to the 1/rev rotor tach signal.
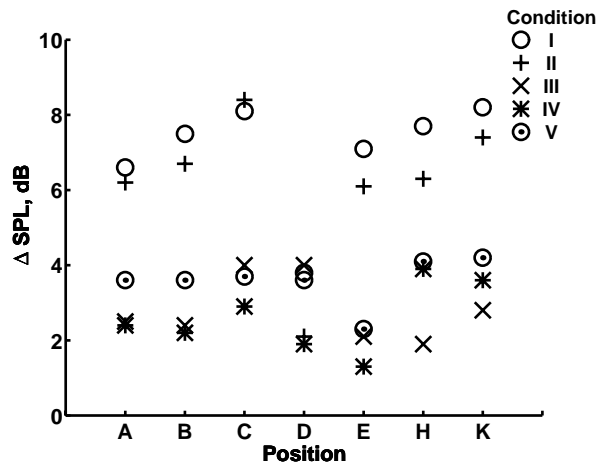
Figure 13. Difference in measured and predicted spectral levels averaged across frequency.

In order to provide a loading function for structural acoustic predictions, the complex spatial pressure must be well predicted. Here the magnitude and phase of the transfer function for each position relative to Position A is compared in Figure 14 and Figure 15, respectively. The plotted values have been calculated by averaging the data for the 5 forward flight conditions. The measured data

presented in Ref. [3] showed that the forward speed has little effect on the magnitude or phase of the transfer functions. Generally, the spatial variation of the magnitude is replicated very well by the predictions. Note that both the measured and predicted data for Position E indicate a higher response at E than at A, indicating that Position E is closer to the rotor. In addition, the magnitude significantly decreases at the higher frequencies moving aft of the propeller plane, Positions B-D, as was noted for the autospectra. The phase is also well replicated by the predictions. The primary difference in trend is noted for Position E where the measured phase appears nearly flat as a function of frequency, while the predicted phase increases with increasing frequency.

The average difference in measured and predicted magnitude and phase of the transfer function is shown in Figure 16. As for the data presented in Figure 13, the averages were calculated from the absolute value of the differences and include only the results for the frequencies where the measured coherences were greater than 0.5. The predictions reproduced the measured magnitude of the transfer function very well, with average values ranging from 0.2 dB at Position B to 1.5 dB at Position H. The phase correlation was also good with average values ranging from 7 degrees at Position A to 34 degrees at Position H.
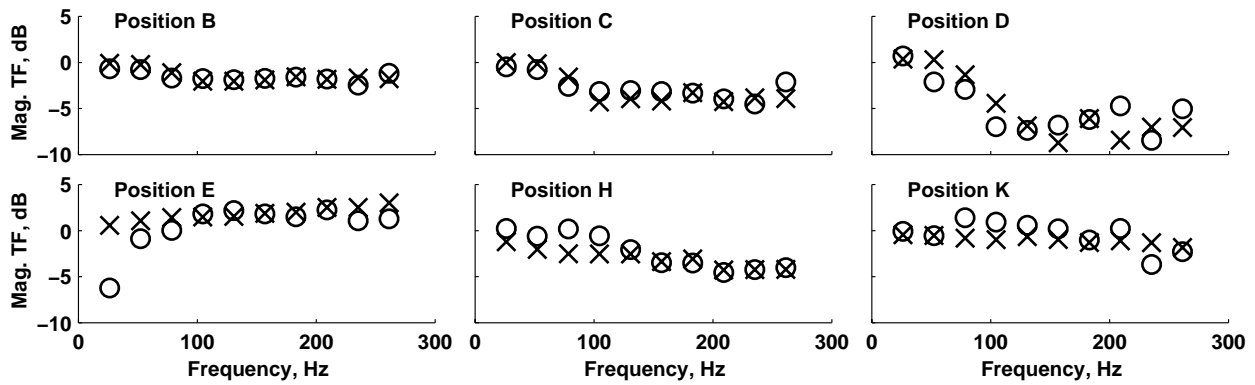
Figure 14. Comparison of measured and predicted average phase of the transfer function relative to the pressure at Position A (measured **O**, predicted ×).
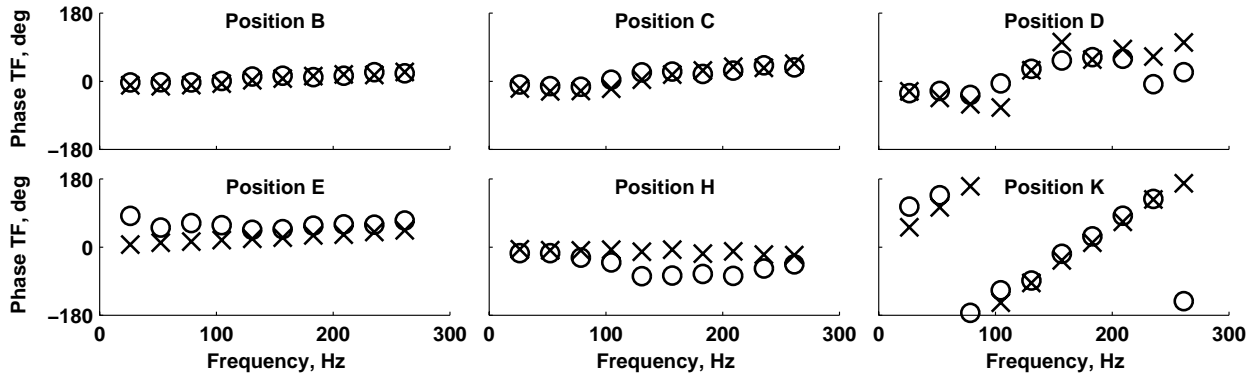
Figure 15. Comparison of measured and predicted average phase of the transfer function relative to the pressure at Position A (measured **O**, predicted ×).
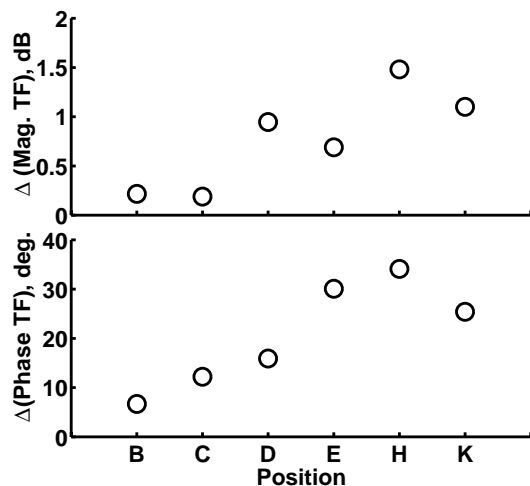
Figure 16. Difference in measured and predicted transfer function averaged across frequency and condition number.

Overall Results

The difference in measured and predicted total levels have been plotted in Figure 17. These total levels were calculated by summing across frequency on an energy basis. Note the smaller variations here, as compared to the data in Figure 13, can be attributed to cancellation of positive and negative differences. In particular, good agreement between measurements and predictions is shown for Positions A to D.
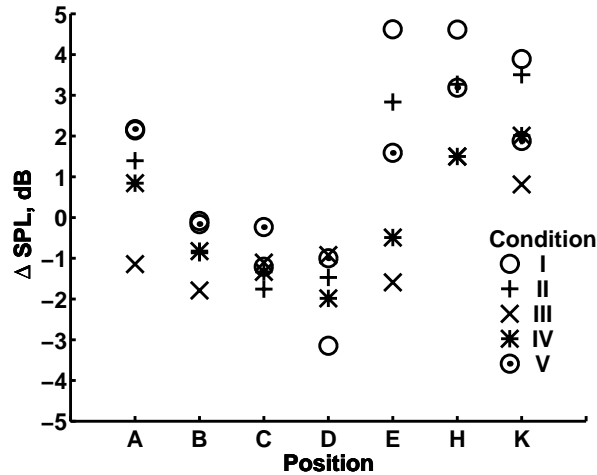
Figure 17. Difference between measured and predicted total SPL based on summing across frequency ($SPL_{meas} - SPL_{pred}$).

Concluding Remarks

Exterior surface acoustic pressure measurements were taken aboard an XV-15 aircraft. The test conditions included level flight in airplane mode for speeds ranging from 72 m/s to 113 m/s. Predictions based on the flight conditions were calculated and compared to the measured data in both the time and frequency domains. The predictions were generated by the TRAC system. The comparisons between measured and predicted data presented in this paper are the first publication of such comparisons for a tiltrotor in airplane mode using TRAC. The following conclusions were drawn from the results:

1) In general, the predictions reproduced the measured data well for Conditions III through V. The correlation for the lower flight speeds, Conditions I and II, was fair. However, the first 3 harmonics for all the positions and flight conditions was well predicted. The average spectral difference between measured and predicted data ranged from 1.3 to 8.4 dB. At the higher harmonics these comparisons were considered surprisingly good considering the number of approximations and assumptions in the modeling.

2) The transfer function data showed very good agreement between measured and predicted results, indicating that the predictions did very well at predicting the spatial variation (both magnitude and phase). The better agreement relative to the spectral comparisons probably results from the nullification of the scattering effects.

3) Discrepancies between the measured and predicted data were noted where the measured data were not well correlated to the tach signal. Since the predictions are based solely on the rotor aeroacoustics, poor correlation between measurements and predictions at these points could be anticipated.

4) The predicted surface pressures were very sensitive to the CFD grid used, including distance from the blade to the transducer, the grid spacing, and position of the branch cut.

5) The measured and predicted surface pressures indicate that for these conditions the nearfield thickness noise is the predominant noise-generating mechanism of the rotor.

In summary, the good correlation of the spatial variation of pressures suggest that a free-field rotor code could be used to predict the surface pressures on a tiltrotor for input to a structural acoustic model designed for interior noise parametric studies. The initial TRAC predictions for airplane mode conditions show promise; however, further refinements and validation are necessary. Caution needs to be exercised in extrapolating these results to other flight conditions, since the unusually good correlation was not expected due to the simplifying assumptions and approximations of the model.

[1] Shank, S. "Tiltrotor Interior Noise Characteristics" Proceedings American Helicopter Society/Royal Aeronautical Society Technical Specialists' Meeting on Rotorcraft Acoustics and Rotor Fluid Dynamics, Philadelphia, PA, October 15-17, 1991.

[2] Maisel, M., principal investigator, US Army AATD, private correspondence, 1983.

[3] Lyle, K. H. "XV-15 Structural-Acoustic Data" NASA TM-112855/U.S. Army Research Laboratory TR-1423, June 1997.

[4] Burley, C. L., Marcolini, M. A., Brooks, T. F., Brand, A., G., Conner, D. A., "Tiltrotor Aeroacoustic Code (TRAC) Predictions and Comparison with Measurements," AHS 52nd Annual Forum Technology Display, 1996.

[5] Brooks, T. F., Boyd, D. D., Burley, C. L. and Jolly, R. J., "Aeroacoustic Codes for Rotor Harmonic and BVI Noise - CAMRAD.Mod1/HIRES," AIAA Paper No. 96-1735, 1996.

[6] Johnson, W., "A Comprehensive Analytical Model of Rotorcraft Aerodynamics and Dynamics," NASA TM 81182, June 1980.

[7] Prichard, D. S., Boyd, D. D., and Burley, C. L., "NASA/Langley's CFD-Based BVI Rotor Noise Prediction System: (ROTONET/FPRBVI) An Introduction and User's Guide," NASA TM 109147, November, 1994.

[8] Strawn, R. C., and Caradonna, F. X., " A Conservative Full-Potential Model for Unsteady Transonic Rotor Flow," AIAA Journal, Vol. 25, February, 1987.

[9] Johnson, W., "An Assessment of the Capability To Calculate Tilting Prop-Rotor Aircraft Performance, Loads, and Stability," NASA TP 2291, 1984.

[10] Bell Helicopter Company, "Advancement of Proprotor Technology - Wind Tunnel Test Results,," NASA CR-114363, September 1971.

[11] Bridgeman, J. O., Prichard, D., and Caradonna, F. X., "The Development of a CFD Potential Method for the Analysis of Tilt-Rotors", Presented at AHS Technical Specialists Meeting on Rotorcraft Acoustics and Fluid Dynamics, Philadelphia, PA, October 15-17, 1991.